electronics

MDPI

Article

Instantaneous Overcurrent Protection for Active Distribution Networks Considering Photovoltaic Fault Current Contribution

Zhui Wei [1], Yongjie Wang [2,*], Jiajing Kong [2], Chi Li [2], Kai Sun [1], Yinghui Xu [1], Rui Guo [1] and Lingyan Sun [1]

[1] State Grid Shandong Electric Power Company Liaocheng Power Supply Company, Liaocheng 252022, China; 13210958055@163.com (Z.W.); sgccsunk@163.com (K.S.); xuyinghui0925@163.com (Y.X.); zhongguo20031015@126.com (R.G.); 20604010004@stumail.sdut.edu.cn (L.S.)

[2] State Key Laboratory of Alternate Electrical Power System with Renewable Energy Sources, North China Electric Power University, Beijing 102206, China; kjj20100304@126.com (J.K.); lichi_ncepu@163.com (C.L.)

* Correspondence: wangelectrique@ncepu.edu.cn

Abstract

Fault-current contributions from high-penetration distributed photovoltaic (PV) generation can extend the reach of instantaneous overcurrent protection. However, increasing the current pickup to maintain selectivity may conflict with relay setting limits, current transformer (CT) constraints, and near-end fault sensitivity requirements, leaving no feasible current-only setting. To address this problem, an instantaneous overcurrent protection setting method considering PV fault current contributions is proposed. Using the complementary variations in the protection reaches of the current and voltage elements with system operating conditions, a combined current–voltage protection reach model is established, and the settings of the two elements are coordinated to maximize the aggregate protection reach while satisfying selectivity and current capability constraints. A unified feasible setting region is further established to efficiently determine the optimal setting combination. The case study results show that, under operating conditions in which conventional instantaneous overcurrent protection cannot simultaneously satisfy selectivity and current capability constraints, the proposed method can still obtain implementable settings, ensure reliable blocking for external faults, and retain instantaneous protection for near-end faults.

Keywords: instantaneous overcurrent protection; distributed photovoltaic generation; undervoltage supervision; protection reach; relay setting optimization; discrete voltage settings

Academic Editor: Herminio Martínez-García

Received: 2 November 2026
Revised: 23 November 2026
Accepted: 27 November 2026
Published: 29 November 2026

Copyright: © 2026 by the authors. Licensee MDPI, Basel, Switzerland. This article is an open access article distributed under the terms and conditions of the Creative Commons Attribution (CC BY) license.

1. Introduction

The increasing integration of distributed photovoltaic (PV) generation affects power system operation under different renewable penetration levels, including voltage regulation and supply continuity [1], while also changing the fault characteristics of distribution networks. A network that was originally supplied radially from a single upstream source may now receive fault current from several locations. These changes can impair the dependability, sensitivity, and selectivity of conventional multistage overcurrent protection [2–4].

The effects of distributed PV integration differ among the stages of multistage overcurrent protection. Specifically, time-delayed high-set overcurrent protection and

definite-time overcurrent protection are relatively less affected by PV fault current contributions, and their selectivity is primarily ensured through operating-time coordination. In contrast, instantaneous overcurrent protection operates without an intentional time delay, and PV fault current contributions may directly extend its protection reach, resulting in nonselective tripping. Therefore, instantaneous overcurrent protection is more sensitive to PV fault current contributions, making its setting determination particularly important [5,6].

Existing approaches to improving distribution protection can be broadly classified into two categories: distributed protection using external information and improvements to local protection relying solely on local information [7]. The former benefits from access to external information and can adapt relay settings to changes in network topology and DG status [8]. However, their deployment may be constrained by communication infrastructure, implementation costs, and the requirements of existing distribution networks [9]. These limitations motivate further improvements to conventional local overcurrent protections.

Conventional protection-setting calculations for active distribution networks generally adopt one of two approaches. In the first approach, distributed PV systems are treated as loads, and protection settings are still calculated by assuming a single-source radial network, making it difficult to accommodate PV integration and leading to poorer selectivity and reduced sensitivity at different protection levels [10]. In the second approach, the effects of distributed PV are considered on a worst-case basis, i.e., under the most extreme conditions. Although this approach provides a conservative basis for selectivity, the resulting current pickup may exceed practical setting limits, leaving no feasible current-only setting [11]. Several studies have addressed these issues. References [12–15] attempt to recalculate fault quantities online based on the operating state and update current protection settings in real time, thereby maintaining overcurrent protection settings within a feasible range. However, their implementation generally requires information on the current network state, DG operating parameters, or online calculation results, imposing corresponding requirements on state-information acquisition, communication, and online setting capabilities. Voltage information has also been incorporated into overcurrent operating characteristics to improve relay coordination and operating speed [16]. Composite current-impedance criteria have also been investigated to mitigate PV-induced protection reach extension in instantaneous protection [17]. The measured impedance can also be affected by inverter control characteristics, motivating adaptive correction in impedance-based protection [18].

Voltage elements have been widely used in generator backup overcurrent protection, providing a reference for using voltage information to improve overcurrent protection performance [19]. This paper addresses the setting determination of instantaneous overcurrent protection considering current capability constraints. The proposed method enables feasible settings to be obtained when conventional current-only protection cannot simultaneously satisfy selectivity and current capability requirements, while retaining instantaneous protection for near-end faults. It further provides globally optimal setting combinations under the prescribed operating conditions and practical discrete voltage setting constraints. The case study results demonstrate the validity and effectiveness of the proposed method.

https://doi.org/10.3390/electronics15235605

2. Modeling and Optimization of Instantaneous Overcurrent Protection Settings

2.1. Influence of PV Generation on Instantaneous Overcurrent Protection

Distributed PV generation changes the distribution of short-circuit currents and can therefore affect both the selectivity and the feasibility of instantaneous overcurrent settings. The following analysis first identifies the additional current seen by the feeder relay and then establishes the constraint imposed by its maximum allowable current pickup.

2.1.1. Additional Fault Current Seen by the Feeder Relay

In a conventional radial distribution network, the upstream system supplies most of the short-circuit current. The current measured at the feeder relay generally decreases as the electrical distance to the fault increases. The instantaneous current pickup is consequently selected to exceed the maximum current associated with a fault at the intended external protection boundary. After PV integration, the aggregate contribution of many current-limited inverters can still alter protection coordination. The effect depends on their connection locations and the network configuration as well as their aggregate capacity [20].

Consider the arrangement in Figure 1, where PV1 is connected to another feeder on the same bus as the protected feeder. For a fault near the first downstream circuit breaker outside the substation, both the upstream system and PV units on the other feeders can supply current through the protected feeder circuit breaker. The PV contribution passing through the relay increases the fault current that it measures. This is the fault current augmentation considered in this study. Unlike PV1, PV2 and PV3 are located on the protected feeder, where their effects on the current measured at DL depend on their positions relative to the fault.

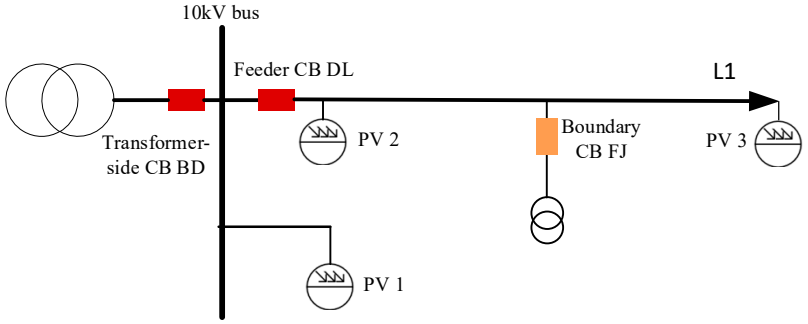


Figure 1. Typical configuration of an active distribution network.

The fault current at the relay can be expressed as

$$I_f = I_s + \Delta I_{NE} \quad (1)$$

where I_f is the measured fault current, I_s is the contribution from the upstream system, and ΔI_{NE} is the additional contribution from distributed PV generation. For setting calculations, the fault-current contribution from PV units on other feeders is determined by their aggregate capacity and the current-sharing relationship. The maximum PV fault-current magnitude is expressed as $I_{PV,\,max} = KS_{PV}/(\sqrt{3}U_N)$, where S_{PV} is the aggregate PV capacity, U_N is the nominal line-to-line voltage, and K specifies the assumed inverter fault-current limit used for selectivity-oriented setting and is selected according to the current-limiting characteristics of the PV units. With the current sharing factor $k = Z_s/(Z_s + Z_f)$, the contribution through DL is bounded by $|\Delta I_{NE}| \le |k| I_{PV,\,max}$. Taking the most unfavorable phase

alignment with the upstream fault current gives the maximum relay current used for selectivity setting.

To prevent operation for a fault at the first downstream sectionalizing, boundary, or branch circuit breaker, the current pickup must satisfy

$$I_{\mathrm{dz,min}} \geq I_{\mathrm{sel}} = K_k I_{f,\max} \tag{2}$$

where K_{k} is the reliability factor, $I_{\mathrm{dz,min}}$ is the minimum pickup required for selectivity, and $I_{\mathrm{f,max}}$ is the maximum fault current measured by the feeder relay at the external boundary, including the PV contribution. A larger PV contribution therefore raises the lower bound on the current pickup.

2.1.2. Setting Feasibility Under Current Capability Constraints

Raising the current pickup can prevent the excessive reach caused by PV generation. In practice, however, the pickup is bounded by the relay setting range, current transformer (CT) constraints, and the required sensitivity to faults immediately downstream of the relay. The maximum allowable current pickup is defined as

$$I_{\mathrm{lim}} = \min\{I_{\mathrm{dev}}, I_{\mathrm{CT}}, I_{\mathrm{sen}}\} \tag{3}$$

where I_{dev}, I_{CT}, and I_{sen} denote the respective current limits. If the minimum pickup required for selectivity exceeds I_{lim}, no current-only setting can satisfy both selectivity and current capability constraints. Additional local information is then needed to restrict the protection reach while retaining operation without an intentional delay.

2.2. Principles of Undervoltage Supervised Instantaneous Overcurrent Protection

An undervoltage element is introduced to supervise the overcurrent element when a current-only setting is infeasible. The voltage element responds to the residual bus voltage during a fault and permits instantaneous operation only when that voltage falls below its threshold. Coordinating the two elements restricts the reach across the range of system operating conditions.

2.2.1. Operating Principle of the Voltage Element

Figure 2 shows the radial equivalent used to calculate the residual bus voltage measured by the voltage transformer (VT) at the 10 kV substation bus.

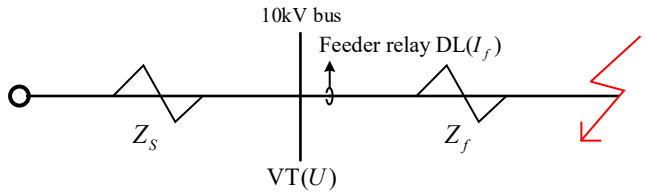


Figure 2. Equivalent circuit for a short circuit on the 10 kV feeder.

For this circuit, let Z_{s} denote the upstream system equivalent impedance and Z_{f} the line impedance between the relay and the fault. Let E denote the line-to-line voltage base on the voltage transformer secondary side. Neglecting fault resistance, the residual voltage at the relay bus is

$$U = \frac{Z_f}{Z_s + Z_f} E \tag{4}$$

where U is the secondary residual bus voltage. For a fixed system equivalent impedance, a more distant fault produces a higher residual voltage. The undervoltage threshold therefore determines the reach of the voltage element.

Let Z_{L} be the line impedance from the feeder circuit breaker to the first downstream circuit breaker that defines the external protection boundary. For a fixed voltage threshold, increasing Z_{s} increases the voltage-element reach. The weak-source condition, represented by $Z_{\mathrm{s,\,max}}$, is therefore used to calculate an initial undervoltage setting at the boundary. Including the reliability factor gives

$$U_{\mathrm{dz}} = U / K_k = \frac{Z_L}{K_k (Z_{s\max} + Z_L)} E \tag{5}$$

The voltage-element reach is smaller under the strong-source condition and larger under the weak-source condition. This dependence is opposite to that of the overcurrent element and is the basis for coordinating their settings.

2.2.2. Combined Current and Voltage Reach Model

Let $U_{\varphi\varphi}$ denote the primary system line-to-line voltage. For a three-phase bolted fault in the adopted radial equivalent circuit, the current measured by the relay is

$$I_f = \frac{U_{\varphi\varphi}}{\sqrt{3}(Z_s + Z_f)} \tag{6}$$

Setting the fault current equal to the current pickup I_{dz} yields the current-element reach

$$Z_I(Z_s) = \frac{U_{\phi\phi}}{\sqrt{3} I_{\mathrm{dz}}} - Z_s \tag{7}$$

Similarly, setting the secondary residual voltage equal to the undervoltage threshold U_{dz} yields the voltage-element reach

$$Z_U(Z_s) = \frac{U_{\mathrm{dz}}}{E - U_{\mathrm{dz}}} Z_s \tag{8}$$

The two elements are combined through AND logic: the current must exceed its pickup and the residual voltage must be below its threshold. The effective combined reach is therefore the smaller of the two element reaches, truncated at zero:

$$Z_{I-U}(Z_s) = \max[0, \min\{Z_I, Z_U\}] \tag{9}$$

Consequently, a voltage sag alone cannot initiate operation when the feeder current remains below its pickup. In practical implementation, the combined criterion operates after both measured conditions are satisfied, without introducing an additional intentional coordination delay.

For the radial fault path represented in Figure 2, with no intermediate current injection between DL and the fault, the bus phase voltage satisfies the following relationship: $U_{\mathrm{bus,\,ph}} = I_f Z_f$. Since the current and voltage elements must operate simultaneously, their operating conditions are $I_f \geq I_{\mathrm{dz}}$ and $U \leq U_{\mathrm{dz}}$. Accordingly, the fault-path impedance is bounded by

$$|Z_f| \leq \frac{U_{\mathrm{dz}}}{E} \cdot \frac{U_{\varphi\varphi}}{\sqrt{3} I_{\mathrm{dz}}} \tag{10}$$

This relationship indicates that voltage supervision constrains the instantaneous protection reach even when PV penetration on other feeders increases the fault current measured at DL.

As illustrated in Figure 3, three reach regimes are possible. If the current-element reach is smaller throughout the operating interval, the current element limits the protection reach. If the voltage-element reach is smaller throughout the interval, the voltage element limits the reach. If the curves intersect within the interval, the voltage element limits the reach for some system conditions and the current element limits it for the remaining conditions.

https://doi.org/10.3390/electronics15235605

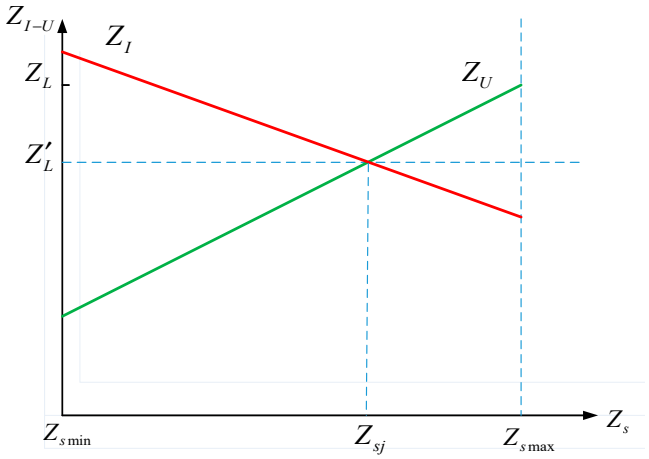


Figure 3. Combined protection reach and the intersection of the current and voltage reach curves over the system impedance interval.

2.2.3. Current–Voltage Coordinated Setting Procedure

The coordinated setting procedure first calculates the current pickup required by conventional instantaneous overcurrent selectivity. Including the contribution from PV generation on other feeders of the same bus gives

$$I_{\mathrm{dz0}} = K_k(I_s + \Delta I_{\mathrm{NE}}) \tag{11}$$

where I_{dz0} is the conventional pickup and the upstream contribution at the boundary under the strong-source condition is

$$I_s = \frac{U_{\varphi\varphi}}{\sqrt{3}(Z_{s\min} + Z_L)} \tag{12}$$

Here, $Z_{\mathrm{s,min}}$ is the minimum system equivalent impedance. The calculated pickup is then checked against the relay setting limit, the CT-related limit, and the sensitivity requirement for a bolted fault immediately downstream of the relay. If all checks are satisfied, the current-only instantaneous stage can be retained. Otherwise, its current pickup must be reduced and the voltage element enabled to restrict the reach.

One construction for coordinating the elements places the intersection of their reach curves at the reduced design boundary

$$Z'_L = \frac{Z_L}{K_k} \tag{13}$$

The system impedance at the intersection and the corresponding current pickup are then given by

$$Z_{\mathrm{sj}} = \frac{Z_L}{K_k}\frac{E - U_{\mathrm{dz}}}{U_{\mathrm{dz}}} \tag{14}$$

$$I_{\mathrm{dz}} = \frac{K_k U_{\varphi\varphi} U_{\mathrm{dz}}}{\sqrt{3} E Z_L} \tag{15}$$

To compare settings across operating conditions, the area under the combined reach curve over the system impedance interval is used as the objective. When the two curves intersect within that interval, the area can be written as

$$S = \int_{Z_{s\min}}^{Z_{\mathrm{sj}}} Z_U \,\mathrm{d}Z_s + \int_{Z_{\mathrm{sj}}}^{Z_{s\max}} Z_I \,\mathrm{d}Z_s \tag{16}$$

where Z_{sj} is the system impedance at the intersection. This area, denoted by S, aggregates the protection reach across the adopted system impedance interval and has units of square ohms. For fixed line parameters, a larger reach impedance corresponds to a longer feeder

section covered by instantaneous protection. Thus, this objective reflects the aggregate instantaneous protection coverage across the considered system impedance interval.

The procedure then searches for the largest area. If it finds no usable pair in the joint-setting stage, it selects a current pickup from the near-end three-phase bolted-fault current, the relay setting limit, and the CT-related limit, and relies on the voltage element to limit the reach:

$$I_{\mathrm{dz}} = \min\{I_f, I_{\mathrm{dev}}, I_{\mathrm{CT}}\} \tag{17}$$

This coordinated procedure provides engineering settings under different current capability constraints. The following analysis further accounts for discrete voltage settings and compares the feasible solutions across different protection reach regimes. An empty set of available voltage steps does not necessarily mean that the corresponding continuous interval is empty. Moreover, fixing the curve intersection at the design boundary is only one way to satisfy the reach constraint. The optimization below therefore compares feasible settings across all three reach regimes.

2.3. Setting Optimization with Discrete Voltage Thresholds

Practical relays provide settings in prescribed increments. The analysis explicitly accounts for the voltage setting step while treating the current pickup as continuous within its allowable range. It first tests the feasibility of the joint-setting interval and then constructs a finite candidate set over the unified current and voltage feasible region.

2.3.1. Feasibility of Discrete Voltage Settings

In the joint-setting construction, the current and voltage reach curves intersect at the design boundary, and the intersection must lie between the strong-source and weak-source operating conditions. These requirements establish the lower and upper voltage thresholds

$$\underbrace{\frac{EZ_L}{K_k Z_{s\max} + Z_L}}_{U_{\mathrm{dz\,min}}} \le U_{\mathrm{dz}} \le \underbrace{\frac{EZ_L}{K_k Z_{s\min} + Z_L}}_{U_{\mathrm{dz\,max}}} \tag{18}$$

The allowable current pickup imposes an additional upper bound on the voltage setting:

$$U_{\mathrm{dz}} \le U_I = \frac{\sqrt{3} E Z_L I_{\mathrm{lim}}}{K_k U_{\varphi\varphi}} \tag{19}$$

Combining these constraints with the relay voltage setting range gives the continuous feasible interval

$$U_{\mathrm{dz}} \in [L, H] \tag{20}$$

Its endpoints are defined by

$$\begin{aligned} L &= \max\{U_{\min}, U_{\mathrm{dz\,min}}\} \\ H &= \min\{U_{\max}, U_{\mathrm{dz\,max}}, U_I\} \end{aligned} \tag{21}$$

Let ΔU denote the voltage setting step. For the zero-offset voltage grid used here, the interval contains an implementable setting if and only if

$$\left\lceil \frac{L}{\Delta U} \right\rceil \le \left\lfloor \frac{H}{\Delta U} \right\rfloor \tag{22}$$

A continuous interval can thus be nonempty while containing no available voltage setting. Such a result identifies the absence of a candidate in that joint-setting interval; it does not establish that the complete setting problem is infeasible or that a particular alternative reach regime must be selected.

2.3.2. Finite Candidate Solution in the Joint-Setting Region

With the intersection fixed at the design reach, the voltage threshold and current pickup are coupled. Using the system impedance at the intersection as the optimization variable gives

$$\begin{cases} U_{\mathrm{dz}} = \dfrac{EZ_L}{K_k Z_{\mathrm{sj}} + Z_L} \\ I_{\mathrm{dz}} = \dfrac{U_{\varphi\varphi}}{\sqrt{3}(Z_{\mathrm{sj}} + Z_L / K_k)} \end{cases} \tag{23}$$

Each admissible intersection impedance therefore corresponds to one setting pair. Define Z_{a} as the line boundary impedance divided by the reliability factor. The element reach curves become

$$\begin{cases} Z_U(Z_s) = \dfrac{Z_a Z_s}{Z_{\mathrm{sj}}} \\ Z_I(Z_s) = Z_{\mathrm{sj}} + Z_a - Z_s \end{cases} \tag{24}$$

For an interior intersection and an integration interval over which the current reach remains nonnegative, the area in Equation (15) can be rewritten as

$$S = \int_{Z_{s\min}}^{Z_{\mathrm{sj}}} \frac{Z_a}{Z_{\mathrm{sj}}} Z_s \,\mathrm{d}Z_s + \int_{Z_{\mathrm{sj}}}^{Z_{\mathrm{smax}}} (Z_{\mathrm{sj}} + Z_{\mathrm{a}} - Z_{\mathrm{s}})\mathrm{d}Z_{\mathrm{s}} \tag{25}$$

Integration yields

$$S = \frac{Z_a}{2}\left(Z_{\mathrm{sj}} - \frac{Z_{s\min}^2}{Z_{\mathrm{sj}}}\right) + \frac{1}{2}(Z_{\mathrm{sj}} + 2Z_a - Z_{\mathrm{s\,max}})(Z_{\mathrm{s\,max}} - Z_{\mathrm{sj}}) \tag{26}$$

The first and second derivatives are

$$\begin{aligned} \frac{\mathrm{d}S}{\mathrm{d}Z_{\mathrm{sj}}} &= Z_{s\max} - Z_{\mathrm{sj}} - \frac{Z_a}{2} + \frac{Z_a Z_{s\min}^2}{2Z_{\mathrm{sj}}^2}, \\ \frac{\mathrm{d}^2 S}{\mathrm{d}Z_{\mathrm{sj}}^2} &= -1 - \frac{Z_a Z_{s\min}^2}{Z_{\mathrm{sj}}^3} < 0 \end{aligned} \tag{27}$$

Under these analytical conditions, the objective is strictly concave in the intersection impedance. The unconstrained continuous optimum satisfies the cubic stationary-point equation

$$2Z_{\mathrm{sj0}}^3 + (Z_a - 2Z_{s\,\max})Z_{\mathrm{sj0}}^2 - Z_a Z_{s\min}^2 = 0 \tag{28}$$

The analytical solution and its conversion to a voltage setting are given in Appendix B. After restricting the continuous optimum to the feasible interval, only the nearest available voltage on either side needs to be evaluated in the joint-setting region. The corresponding current pickups follow from Equation (22), and their combined reach areas are compared.

2.3.3. Unified Feasible Region for the Three Reach Regimes

The joint-setting construction is sufficient to keep the combined reach within the design boundary, but it is not the only admissible construction. A voltage-limited or current-limited setting may also meet the reach constraint even if the intersection lies outside the system operating interval. All three regimes are therefore included in the optimization.

For every system operating condition, the combined reach must not exceed Z_{a}. At any given system impedance, this requires at least one of the current and voltage elements to restrict its own reach to the design boundary. The resulting logical OR condition is

$$\begin{cases} I_{\mathrm{dz}} \geq \dfrac{U\varphi\varphi}{\sqrt{3}(Z_s + Z_a)} \\ U_{\mathrm{dz}} \leq \dfrac{E Z_a}{Z_s + Z_a} \end{cases} \tag{29}$$

Extending this condition over the full system impedance interval gives a piecewise feasible region in the current and voltage setting plane, together with the allowable current limit:

$$\begin{cases} U_{\mathrm{dz}} \leq U_{\mathrm{dz\,min}} \\ I_{\mathrm{dz}} \geq \dfrac{K_k U_{\varphi\varphi}}{\sqrt{3} E Z_L} U_{\mathrm{dz}} & U_{dz\,\mathrm{min}} < U_{dz} < U_{dz\,\mathrm{max}} \\ I_{\mathrm{dz}} \geq \dfrac{U_{\varphi\varphi}}{\sqrt{3}(Z_{s\,\mathrm{min}} + Z_L / K_k)} & U_{dz} \geq U_{dz\,\mathrm{max}} \\ 0 < I_{\mathrm{dz}} \leq I_{\mathrm{lim}} \end{cases} \tag{30}$$

In the low-voltage region, the voltage element alone can enforce the reach boundary throughout the operating interval. Its maximum attainable area increases with the voltage threshold, so only the largest allowed discrete voltage in this region needs to be retained. Once the current-element reach is no smaller than the voltage-element reach for every operating condition, further reduction in the current pickup cannot increase the combined area. Equating the two reaches under the weak-source condition gives the boundary of this area plateau:

$$I_V(U_{\mathrm{dz}}) = \frac{U_{\varphi\varphi}}{\sqrt{3} Z_{s\,\mathrm{max}}} \left(1 - \frac{U_{\mathrm{dz}}}{E}\right) \tag{31}$$

For the selected low-voltage candidate, the current pickup is taken as

$$\min\{I_{\mathrm{lim}}, I_V(U_{\mathrm{dz}})\} \tag{32}$$

This choice uses the largest current pickup that attains the same plateau area while satisfying the current capability limit. It therefore provides a consistent representative when several current pickups give the same objective value.

In the intermediate-voltage region, the minimum feasible current follows the coupled relationship analyzed in Section 2.3.2. The two voltage steps adjacent to the bounded continuous optimum provide at most two candidates. In the high-voltage region, enforcing the reach boundary under all system conditions requires

$$I_{\mathrm{dz}} \geq I_B = \frac{U_{\varphi\varphi}}{\sqrt{3}(Z_{s\,\mathrm{min}} + Z_L / K_k)} \tag{33}$$

This region is feasible only if the boundary current I_{B} does not exceed I_{lim}. Once that current boundary is reached, a higher voltage threshold does not increase the maximum achievable area, so one discrete setting near the region boundary is sufficient to represent it.

The low-, intermediate-, and high-voltage regions thus contribute at most one, two, and one candidate pairs, respectively. After checking whether conventional current-only protection is feasible, the proposed procedure compares the feasible candidates using the combined reach objective. Within the stated equivalent model and analytical conditions, this comparison yields the optimal setting pair without enumerating every voltage step. The absence of a candidate in one region does not prevent feasible settings in the other regions from being evaluated.

3. Results

3.1. Test System and Parameter Settings

The case studies use a 10 kV public distribution feeder supplied from a 110 kV substation with the configuration in Figure 1. DL is the feeder circuit breaker whose instantaneous overcurrent stage is being set, and FJ is the nearest downstream circuit breaker that defines the external protection boundary. In the adopted multistage protection arrangement, the instantaneous stage settings are evaluated using three-phase bolted faults, while the existing time-delayed and ground-fault protection functions retain their respective fault-clearing responsibilities.

The main transformer is rated at 63 MVA. The CT at DL has accuracy class 5P20 and a ratio of 500/5 A. The relay permits a maximum primary current setting of 15 kA. The cable unit impedance is 0.1 Ω/km, the primary system line-to-line voltage is 10.5 kV, and the voltage transformer secondary base is 100 V. The reliability factor is 1.3, and the voltage setting step is 1 V. The inverter fault-current coefficient K is set to 1.2 in the numerical cases. Two parameter sets are used to examine engineering setting feasibility and the effect of discrete voltage steps. Additional engineering data and the parameters of both cases are listed in Appendix A.

3.2. Comparison of Instantaneous Overcurrent Setting Schemes

In Case 1, the system equivalent impedances under the strong- and weak-source conditions are 0.45 Ω and 0.58 Ω, respectively. The 1.5 km cable between DL and FJ has an equivalent impedance of 0.15 Ω. The relay, CT, and near-end fault sensitivity constraints impose current limits of 15 kA, 10 kA, and 13.471 kA, respectively. The allowable pickup is therefore 10 kA.

Figure 4 shows the current and voltage feasible region. The two voltage boundaries divide the setting plane into low-, intermediate-, and high-voltage regions. The horizontal line represents the current capability limit, and the sloping line in the intermediate region is the joint-setting boundary. In the low-voltage region, the descending current boundary identifies the area plateau below which a further reduction in pickup cannot improve the combined reach.

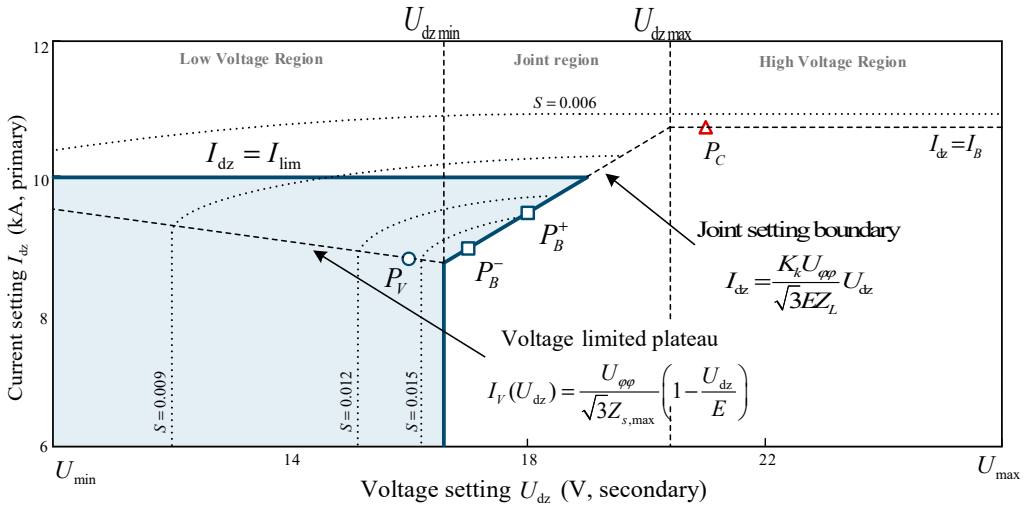


Figure 4. Feasible current and voltage settings for Case 1, including the current capability limit, the joint-setting boundary, and the boundary of the voltage-limited area plateau.

With a 1 V setting step, the largest voltage in the low-voltage region is 16 V. Its current pickup is determined from the plateau boundary, giving candidate P_V. In the intermediate region, the continuous optimal voltage is approximately 17.09 V. Only the

adjacent 17 V and 18 V settings are retained, giving candidates P_B^- and P_B^+. The high-voltage representative P_C is excluded because it violates the current capability limit. The remaining candidates and their objective values are listed in Table 1.

Table 1. Candidate settings and aggregate protection reach areas in Case 1.

Candidate	Voltage (V)	Current (kA)	Area (Ω^2)
P_V	16	8.780	0.01275
P_B^-	17	8.932	0.01355
P_B^+	18	9.457	0.01289

The selected setting is a secondary voltage threshold of 17 V and a primary current pickup of 8.932 kA. Among the feasible candidates in Table 1, this pair gives the largest aggregate reach area.

Three schemes are compared. Scheme 1 determines the current pickup using only the upstream system fault-current contribution, neglecting PV-induced fault current augmentation at the feeder relay [21]. Scheme 2 recalculates the pickup using the maximum fault current including the DG contribution, following the conventional selectivity-setting principle discussed in studies accounting for DG fault currents [22,23]. Scheme 3 is the proposed coordinated current and voltage setting. All schemes are evaluated under the same system parameters and current capability constraints.

The current-only schemes satisfy the selectivity requirement if their pickup is no smaller than the reliability factor multiplied by the maximum fault current at the external boundary. For the coordinated scheme, selectivity is assessed by checking that the voltage element blocks a boundary fault throughout the system operating interval. The current capability check requires the pickup to remain within the relay, CT, and sensitivity limits. Table 2 summarizes the setting and constraint checks.

Table 2. Settings and constraint checks for the three protection schemes.

Scheme	Current (kA)	Voltage (V)	Selectivity	Current Capability
1	13.135	-	Not satisfied	Not satisfied
2	14.421	-	Satisfied	Not satisfied
3	8.932	17	Satisfied	Satisfied

Scheme 1 does not provide the required selectivity margin after PV generation is included. Scheme 2 restores that margin, but its required pickup exceeds the allowable current limit. Both current-only settings therefore fail the combined requirements in this case. Under the conventional configuration, disabling the instantaneous stage would leave fault clearance to time-delayed protection and reduce the ability to clear near-end faults without an intentional delay. Scheme 3 instead uses voltage supervision to restrict the reach while keeping the current pickup within its allowable limit.

3.3. Effect of Discrete Voltage Settings

In Case 2, the system equivalent impedances under the strong- and weak-source conditions are 0.44 Ω and 0.54 Ω, respectively. The cable between DL and FJ is 1 km long and has an equivalent impedance of 0.10 Ω. The relay, CT, and near-end fault sensitivity limits are 15 kA, 10 kA, and 13.777 kA, respectively, giving an allowable current pickup of 10 kA.

The feasible setting region is shown in Figure 5. The continuous joint-setting voltage interval extends from 12.4688 V to 12.6890 V. It is nonempty but contains no voltage available on the 1 V grid, so the intermediate region contributes no implementable candidate.

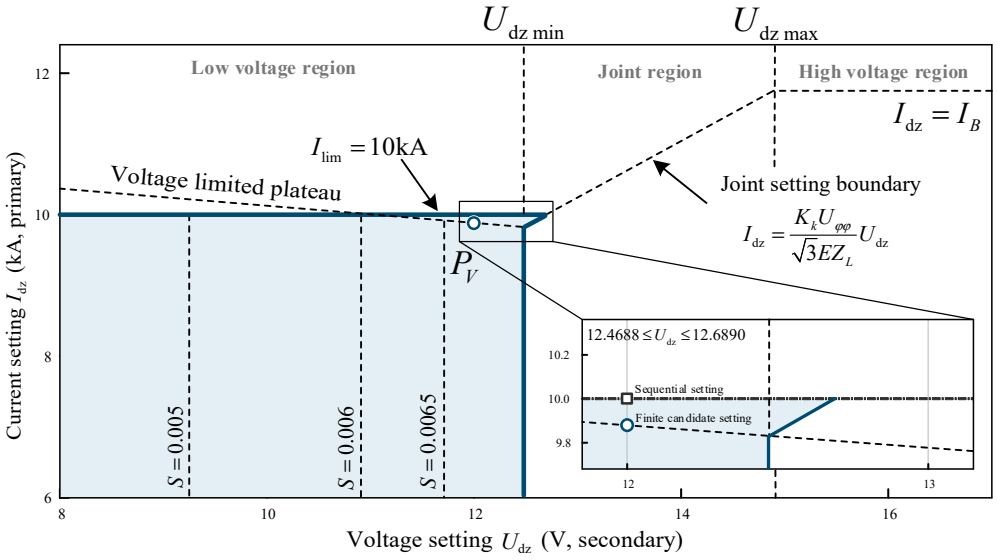


Figure 5. Feasible setting region for Case 2 and an enlarged view of the continuous joint-setting interval that contains no available integer voltage setting.

The sequential engineering procedure then uses a voltage threshold of 12 V and the maximum allowable current pickup of 10 kA, with the voltage element restricting the reach. The proposed procedure continues to evaluate the candidate at 12 V within the complete feasible region. Equating the current and voltage reaches under the weak-source condition gives a plateau-boundary current of 9.8791 kA.

At this current pickup, the two reach curves intersect at the maximum system equivalent impedance. The combined reach has reached the largest value attainable with the 12 V voltage threshold throughout the operating interval. Reducing the current pickup further cannot increase the area. The selected representative is therefore a 12 V voltage threshold and a 9.8791 kA current pickup. The aggregate reach area increases from 6.6576 × 10^{-3} Ω² for the sequential setting to 6.6818 × 10^{-3} Ω² for the proposed setting.

This case shows why an empty discrete joint-setting interval should not directly determine the next branch of the setting procedure. A feasible voltage step outside that interval can still admit a better current pickup. Comparing candidates in the unified feasible region preserves this opportunity and uses the complementary reach characteristics of the two elements.

The finite-candidate optimization method was further compared with exhaustive enumeration over 13,125 parameter combinations. Among the 13,117 feasible cases, both methods obtained identical optimal objective values. The comparison confirms that the finite-candidate method preserves the optimal solution while substantially reducing the number of candidate settings requiring evaluation.

3.4. Validation Under Different PV Capacities and Operating Conditions

To further evaluate the proposed settings, controlled comparisons were conducted using the PSCAD results. Three factors were examined separately: PV capacity, system equivalent impedance, and fault location. In the PV-capacity comparison (Test A), the source impedance and protection settings were fixed. In the source-impedance comparison (Test B), PV capacity was fixed, and the corresponding protection settings were determined for each operating condition. For the fault-location comparison (Test C), the source impedance and PV capacity were fixed at 0.5 Ω and 10 MW, respectively. The fault-location comparison was conducted using a common setting pair. The results are presented in Tables 3 and 4.

Table 3. Relay measurements and protection settings under controlled variations in PV capacity and source impedance.

Test	Z_s (Ω)	PV (MW)	I_{dz} (kA)	U_{dz} (V)	I_{mea}^{DL} (kA)	I_{mea}^{FJ} (kA)	U_{mea}^{FJ} (V)
A	0.5	2	8.932	17	12.233	9.429	23.328
A	0.5	5	8.932	17	12.431	9.581	23.705
A	0.5	10	8.932	17	12.760	9.835	24.333
A	0.5	20	8.932	17	13.419	10.342	25.589
B	0.5	10	8.932	17	12.760	9.835	24.333
B	1.0	10	4.658	10	6.716	5.845	14.463
B	1.5	10	3.106	7	4.698	4.274	10.574
B	2.0	10	2.330	5	3.689	3.433	8.495
B	3.0	10	1.553	3	2.680	2.553	6.316
B	4.0	10	1.165	2	2.175	2.097	5.188

In Table 3, I_{mea}^{DL} denotes the measured fault current near DL, while I_{mea}^{FJ} and U_{mea}^{FJ} represent the measured fault current and residual bus voltage for a fault beyond FJ, respectively. Increasing PV capacity raises both the fault current measured at the feeder relay and the residual bus voltage under fixed network conditions. The voltage element maintains external-fault blocking despite the increased fault current measured at the feeder relay. Variations in source impedance also change the available fault current and the corresponding optimal settings, demonstrating the adaptability of the setting procedure to different source conditions.

Table 4. Current–voltage criterion responses at different fault locations under fixed operating conditions.

Fault Location	Current (kA)	I_{dz} (kA)	Voltage (V)	U_{dz} (V)	Protection	Pickup (ms)
Near DL	12.760	8.932	0.204	17	Operated	9.0
10% of DL-FJ	12.412	8.932	3.072	17	Operated	9.3
20% of DL-FJ	12.061	8.932	5.970	17	Operated	9.6
80% of DL-FJ	10.310	8.932	20.414	17	Blocked	-
Beyond FJ	9.835	8.932	24.333	17	Blocked	-

Table 4 further illustrates the complementary roles of the current and voltage elements. Although the overcurrent condition is satisfied at all five fault locations, the undervoltage element restricts operation to the near-end section. Across the complete set of 120 PSCAD criterion checks, the expected operating and blocking states were obtained. For the 72 operating cases, the AND criterion was first satisfied within 8.4–9.8 ms after fault inception.

3.5. Influence of CT Characteristics on Protection Setting Optimization

To investigate the influence of CT characteristics on protection setting optimization, three representative protection CT configurations, 5P15, 5P20, and 5P30, were selected. The corresponding CT-related current limits were set to 7.5, 10, and 27 kA, respectively. With the other parameters of Cases 1 and 2 unchanged, the current and voltage settings were recalculated under different CT constraints. The CT-related current limit is used as an accuracy-limit-based setting constraint, while transient saturation also depends on the secondary burden, remanence, and fault-current DC offset.

The results presented in Table 5 indicate that the influence of CT capability on protection reach depends on the dominant setting constraint. Relaxing the CT current limit can improve the optimal protection reach, but further increases provide no benefit once other constraints become dominant. Moreover, the coordinated current–voltage criterion allows different current settings to achieve the same protection reach, while changes in the limiting constraint may enable a more favorable voltage setting. Thus, the proposed method makes effective use of available CT capability without requiring unnecessary hardware upgrades.

Table 5. Optimal protection settings under different CT configurations.

Index	Case	CT Class	I_{CT} (kA)	I_{lim} (kA)	I_{dz} (kA)	U_{dz} (V)	Area (Ω^2)
1	1	5P15	7.5	7.5	7.500	16	0.01275
2	1	5P20	10	10	8.932	17	0.01355
3	1	5P30	27	13.471	8.932	17	0.01355
4	2	5P15	7.5	7.5	7.500	12	0.00668
5	2	5P20	10	10	9.879	12	0.00668
6	2	5P30	27	13.777	10.245	13	0.00696

The CT current limits were determined from the representative rated primary currents and their corresponding accuracy-limit factors.

4. Conclusions

Fault current contributions from distributed PV generation can raise the selective current pickup of instantaneous overcurrent protection above the allowable relay, CT, or sensitivity limit. Ignoring that contribution reduces the selectivity margin, whereas increasing the pickup may eliminate the feasible current-only setting interval. Coordinating an overcurrent element with an undervoltage element can resolve this conflict within the adopted equivalent model and retain instantaneous protection for near-end faults.

The current and voltage element reaches vary in opposite directions as the system equivalent impedance changes. A unified feasible region allows voltage-limited, jointly limited, and current-limited settings to be compared under the same reach and current capability constraints. Accounting explicitly for discrete voltage steps prevents an empty joint-setting candidate set from being mistaken for complete infeasibility. The unified optimization reduces the search to a small finite set of candidate setting pairs, avoiding exhaustive enumeration while improving the utilization of the available protection reach. The results also indicate that the proposed settings maintain effective near-end protection while restricting operation for external faults across different operating conditions, with the achievable protection reach depending on the prevailing current capability constraints.

Author Contributions: Writing—original draft preparation, methodology, and formal analysis, Z.W.; writing—review and editing, Z.W. and L.S.; software and validation, Y.W., C.L. and J.K.; data curation, J.K.; project administration and investigation, K.S., Y.X. and R.G. All authors have read and agreed to the published version of the manuscript.

Funding: This research was funded by a grant from the Science and Technology Project of State Grid Shandong Electric Power Company (Grant No. 520611250001).

Data Availability Statement: All data are contained within this article.

Conflicts of Interest: Authors Zhui Wei, Kai Sun, Yinghui Xu, Rui Guo and Lingyan Sun were employed by State Grid Shandong Electric Power Company Liaocheng Power Supply Company. The remaining authors declare that the research was conducted in the absence of any commercial or financial relationships that could be construed as a potential conflict of interest. The authors declare

that this study received funding from the Science and Technology Project of State Grid Shandong Electric Power Company (Grant No. 520611250001). The funder was not involved in the study design, collection, analysis, interpretation of data, the writing of this article or the decision to submit it for publication.

Appendix A. Engineering and Case Parameters

Tables A1 and A2 provide the engineering data and the two parameter sets used in Section 3. Current pickups are referred to the primary side, and voltage thresholds are referred to the voltage transformer secondary side.

Table A1. Engineering parameters of the distribution feeder.

Parameter	Value
Main transformer rating	63 MVA
Rated current on the 10 kV side of the main transformer	3464 A
CT accuracy class	5P20
CT ratio	500/5 A
Cable unit impedance	0.1 Ω/km
Overhead-line unit impedance	0.4 Ω/km
Distribution transformer capacity associated with DL	12,500 kVA
Distribution transformer capacity associated with FJ	630 kVA
Short-circuit impedance of the FJ distribution transformer	10.5 Ω
DG capacity outside the terminal section	2000 kVA
DG capacity at the feeder terminal	500 kVA
DG capacity on other feeders of the same bus	20,000 kVA
Permissible feeder current	540 A

Table A2. Parameters used in the two numerical case studies.

Parameter	Case 1	Case 2
Strong-source system equivalent impedance (Ω)	0.45	0.44
Weak-source system equivalent impedance (Ω)	0.58	0.54
DL–FJ cable length (km)	1.5	1.0
DL–FJ line impedance (Ω)	0.15	0.10
Current limit associated with near-end fault sensitivity (kA)	13.471	13.777

Appendix B. Analytical Solution for the Continuous Optimum

The stationary condition in Section 2.3.2 is expressed in terms of the system impedance at the intersection. With the design reach Z_a equal to the boundary line impedance divided by the reliability factor, the stationary point satisfies

$$2Z_{sj0}^3 + (Z_a - 2Z_{s\max})Z_{sj0}^2 - Z_a Z_{s\min}^2 = 0 \quad \text{(A1)}$$

For the area expression used in the derivation, strict concavity and the endpoint derivative signs give a unique stationary optimum within the system operating interval. The endpoint conditions are

$$S'(Z_{s\min}) > 0, S'(Z_{s\max}) < 0 \quad \text{(A2)}$$

Introduce the coefficients

$$\alpha = \frac{Z_a - 2Z_{s\max}}{2}, \beta = -\frac{Z_a Z_{s\min}^2}{2} \quad \text{(A3)}$$

The stationary equation becomes

$$Z_{sj0}^3 + \alpha Z_{sj0}^2 + \beta = 0 \quad \text{(A4)}$$

A shift in the independent variable gives the depressed cubic

$$y^3 + py + q = 0 \tag{A5}$$

The transformed variable and coefficients are defined by

$$\begin{cases} y = Z_{sj0} + \dfrac{\alpha}{3} \\ p = -\dfrac{\alpha^2}{3} \\ q = \dfrac{2\alpha^3}{27} - \dfrac{Z_a Z_{s\min}^2}{2} \end{cases} \tag{A6}$$

Define the discriminant as

$$\Delta = \left(\frac{q}{2}\right)^2 + \left(\frac{p}{3}\right)^3 \tag{A7}$$

When the discriminant is nonnegative, Cardano's formula gives the real-valued expression

$$Z_{sj0} = -\frac{\alpha}{3} + \sqrt[3]{-\frac{q}{2} + \sqrt{\Delta}} + \sqrt[3]{-\frac{q}{2} - \sqrt{\Delta}} \tag{A8}$$

The cube roots in this expression are real cube roots. The solution used for setting optimization must lie within the applicable operating interval.

The optimal continuous intersection impedance is converted to the unconstrained voltage threshold through

$$U_{dz0} = \frac{EZ_a}{Z_{sj0} + Z_a} \tag{A9}$$

The derivative of the voltage threshold with respect to the intersection impedance is negative:

$$\frac{\mathrm{d}U_{dz}}{\mathrm{d}Z_{sj}} = -\frac{EZ}{(Z_{sj} + Z_a)^2} < 0 \tag{A10}$$

The voltage threshold and intersection impedance therefore have a one-to-one relationship. Restricting the continuous optimal voltage to the feasible interval gives

$$U_{dz}^* = \min\{H, \max(L, U_{dz0})\} \tag{A11}$$

Let the allowed voltage settings form the set $\mathcal{U}$. The candidate immediately below the bounded continuous optimum and the candidate immediately above it are defined by

$$\begin{cases} U_{dz}^- = \max\{U \in \mathcal{U} \cap [L, H] \mid U \le U_{dz}^*\} \\ U_{dz}^+ = \min\{U \in \mathcal{U} \cap [L, H] \mid U \ge U_{dz}^*\} \end{cases} \tag{A12}$$

Only candidates that exist within the feasible interval are retained. If the bounded optimum is itself an allowed voltage, the two definitions identify the same candidate and it is evaluated once. Their associated current pickups and combined reach areas are then calculated as described in Section 2.3.2.

References

1. Hussan, U.; Hassan, M.; Ayub, M.A.; Peng, J.; Rasheed, H.; Jiang, H.; Asghar, F. Smooth and Uninterrupted Operation of Standalone DC Microgrid Under High and Low Penetration of RESs. *IEEE Access* **2024**, *12*, 48620–48629.
2. Al-Baghdadi, A.G.; Abd, M.K.; Flaih, F.M.F. A New Detection Method for Load Side Broken Conductor Fault Based on Negative to Positive Current Sequence. *Electronics* **2022**, *11*, 836.
3. Jimenez, S.; Vázquez, E.; Gonzalez-Longatt, F. Methodology of Adaptive Instantaneous Overcurrent Protection Setting. *Electronics* **2021**, *10*, 2754.
4. Chandraratne, C.; Naayagi Ramasamy, T.; Logenthiran, T.; Panda, G. Adaptive Protection for Microgrid with Distributed Energy Resources. *Electronics* **2020**, *9*, 1959.

5. Li, J.; Feng, J.; Huang, M.; Liu, S.; Wang, G. Optimal protection coordination for directional overcurrent relays in radial distribution networks with inverter-based distributed energy resources. *Int. J. Electr. Power Energy Syst.* **2025**, *167*, 110622.
6. Chen, Z.; Gan, K.; Li, T.; Ruan, W.; Ye, M.; Xu, Q.; Pan, J.; Li, Y.; Liu, C. An Optimized Method for Setting Relay Protection in Distributed PV Distribution Networks Based on an Improved Osprey Algorithm. *Energies* **2026**, *19*, 24.
7. Kennedy, J.; Ciufo, P.; Agalgaonkar, A. A review of protection systems for distribution networks embedded with renewable generation. *Renew. Sustain. Energy Rev.* **2016**, *58*, 1308–1317.
8. Ghotbi-Maleki, M.; Chabanloo, R.M.; Zeineldin, H.H.; Hosseini Miangafsheh, S.M. Design of Setting Group-Based Overcurrent Protection Scheme for Active Distribution Networks Using MILP. *IEEE Trans. Smart Grid* **2021**, *12*, 1185–1193.
9. Coffele, F.; Booth, C.; Dyśko, A. An adaptive overcurrent protection scheme for distribution networks. *IEEE Trans. Power Deliv.* **2015**, *30*, 561–568.
10. Perera, N.; Rajapakse, A.D.; Buchholzer, T.E. Isolation of faults in distribution networks with distributed generators. *IEEE Trans. Power Deliv.* **2008**, *23*, 2347–2355.
11. Ravikumar Pandi, V.; Zeineldin, H.H.; Xiao, W. Determining optimal location and size of distributed generation resources considering harmonic and protection coordination limits. *IEEE Trans. Power Syst.* **2013**, *28*, 1245–1254.
12. Ma, J.; Wang, X.; Zhang, Y.; Yang, Q.; Phadke, A.G. A novel adaptive current protection scheme for distribution systems with distributed generation. *Int. J. Electr. Power Energy Syst.* **2012**, *43*, 1460–1466.
13. Ma, J.; Liu, J.; Deng, Z.; Wu, S.; Thorp, J.S. An adaptive directional current protection scheme for distribution network with DG integration based on fault steady-state component. *Int. J. Electr. Power Energy Syst.* **2018**, *102*, 223–234.
14. Shih, M.Y.; Conde, A.; Leonowicz, Z.M.; Martirano, L. An adaptive overcurrent coordination scheme to improve relay sensitivity and overcome drawbacks due to distributed generation in smart grids. *IEEE Trans. Ind. Appl.* **2017**, *53*, 5217–5228.
15. Cuero-Grueso, J.; Herrera-Orozco, A.; Mora-Flórez, J. Protection strategy for ADN based on overcurrent relay with adaptability unit using local measurements. *Results Eng.* **2025**, *25*, 104410.
16. Saleh, K.A.; Zeineldin, H.H.; Al-Hinai, A.; El-Saadany, E.F. Optimal coordination of directional overcurrent relays using a new time-current-voltage characteristic. *IEEE Trans. Power Deliv.* **2015**, *30*, 537–544.
17. Wei, M.; Wang, C.; Yu, Y.; Liang, Y.; Wang, X. Optimal Configuration Scheme of Multi-staged Protection in Distribution Network for Integration of High Proportion of Distributed Photovoltaic. *Autom. Electr. Power Syst.* **2023**, *47*, 55–65. (In Chinese)
18. Mishra, P.; Pradhan, A.K.; Bajpai, P. Adaptive distance relaying for distribution lines connecting inverter-interfaced solar PV plant. *IEEE Trans. Ind. Electron.* **2021**, *68*, 2300–2309.
19. Ventruella, D.J.; Steciuk, P.B. A second look at generator 51-V relays. *IEEE Trans. Ind. Appl.* **1997**, *33*, 848–856.
20. Bhattacharya, S.; Saha, T.; Hossain, M.J. Fault contribution from large photovoltaic systems in building power supply networks. *J. Build. Eng.* **2016**, *5*, 222–230.
21. Hatefi Torshizi, N.; Najafi, H.; Saberi Noghabi, A.; Sadeh, J. An adaptive characteristic for overcurrent relays considering uncertainty in presence of distributed generation. *Int. J. Electr. Power Energy Syst.* **2021**, *128*, 106688.
22. Ghotbi-Maleki, M.; Chabanloo, R.M.; Taheri, M.R.; Zeineldin, H.H. Coordination of non-directional overcurrent relays and fuses in active distribution networks considering reverse short-circuit currents of DGs. *IET Gener. Transm. Distrib.* **2021**, *15*, 2539–2553.
23. Chen, X.; Li, Y.; Tan, H.; Zhao, M.; Wen, A.; Liu, N. Adaptive Positive-Sequence Instantaneous Overcurrent Protection for Distribution Networks with Inverter-Interfaced Distributed Generation. *Autom. Electr. Power Syst.* **2015**, *39*, 107–112. (In Chinese)

Disclaimer/Publisher's Note: The statements, opinions and data contained in all publications are solely those of the individual author(s) and contributor(s) and not of MDPI and/or the editor(s). MDPI and/or the editor(s) disclaim responsibility for any injury to people or property resulting from any ideas, methods, instructions or products referred to in the content.